CASL-U-2014-0126-000

Power uprates
and plant life extension

Consortium for Advanced Simulation of LWRs

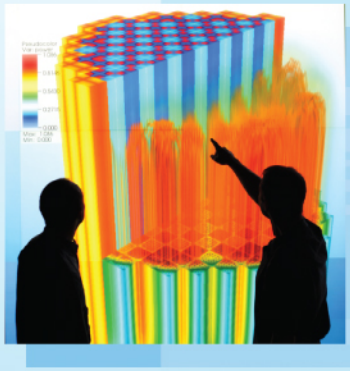

Engineering design
and analysis

L3:MPO.FUEL.P8.01

Pipe Diffusion at Dislocations in UO2

Science-enabling
high performance
computing

Samuel T. Murphy, Eleanor E. Jay,
Robin W. Grimes
Imperial College, London, United
Kingdom

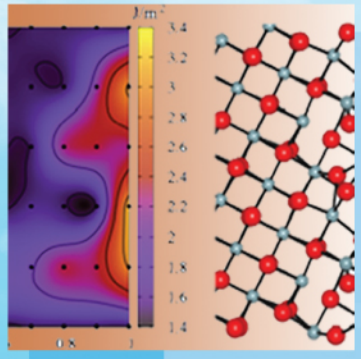

Fundamental science

April, 2014

Plant operational data

U.S. DEPARTMENT OF ENERGY | Nuclear Energy

Journal of Nuclear Materials 447 (2014) 143–149

Contents lists available at ScienceDirect

Journal of Nuclear Materials

journal homepage: www.elsevier.com/locate/jnucmat

Pipe diffusion at dislocations in UO_2

Samuel T. Murphy *, Eleanor E. Jay, Robin W. Grimes

Department of Materials, Imperial College London, South Kensington, London SW7 2BP, UK

ARTICLE INFO

Article history:
Received 5 September 2013
Accepted 30 December 2013
Available online 16 January 2014

ABSTRACT

We present the results of a combination of static and dynamic simulations employing empirical potentials, investigating the structures of dislocations in UO_2 and show how the dislocation core structure influences the rate of O^{2-} and U^{4+} diffusion along the dislocation (i.e. pipe diffusion). In the region immediately surrounding the dislocations there is a significant reduction in the activation energies and diffusion coefficients for O^{2-} and U^{4+} diffusion, however only out to a cylindrical radius of ≈20 Å from the dislocation centre. The contribution of pipe diffusion to the overall O^{2-} and U^{4+} diffusion is also discussed.
© 2014 Elsevier B.V. All rights reserved.

1. Introduction

During its lifetime in-pile nuclear fuel (principally UO_2) is exposed to very high levels of irradiation. One of the most significant consequences is the formation of dislocation loops [1] a process that has been simulated on the atomic scale in UO_2 via molecular dynamics (MD) simulations [2]. As the burn-up of the fuel is increased there is a marked increase in the dislocation density [3], which can have a significant effect on the fuel's properties, for example the creep rate and the thermal conductivity [4]. TEM images of high burn-up fuel pellets show that the dislocations are heavily decorated by fission product precipitates, including gas bubbles and metallic particles [5]. This is consistent with the prediction of a thermodynamic driving force for the segregation of ruthenium [6] and xenon [7] atoms to dislocations using atomistic simulation. At the pellet rim dislocation reorganisation into "sub-boundary" domains caused by dislocations piling up on these fission product precipitates has been proposed as the mechanism responsible for the formation of the high burn-up structure (HBS) [8–10].

The reduced material density near to the core of a dislocation can provide a low energy pathway for migration. Enhanced oxygen conductivity correlated to an increased dislocation density has already been observed in other oxides, for example yttria-stabilized zirconia [11]. Consequently, the increase in dislocation density during the fuel's lifetime may have a significant influence on the rate of oxygen and uranium diffusion through the fuel grain. Dislocations may also provide pathways for enhanced diffusion of fission products, in particular, dislocations pinned to fission product precipitates may enhance the rate at which these bubbles and metallic particles grow. This is particularly important as enhanced diffusion along dislocations may be responsible for the higher than expected rate of Xe diffusion at <1300 K [12].

The breakdown of linear elastic theory close to the dislocation core, coupled to the difficulties encountered in performing direct observations on such a small length scales, means that detailed atomic scale models are useful. A number of theoretical studies have examined pipe diffusion around dislocations in metals [13,14], alloys [15] and ceramics [16], however, no studies of the influence of dislocations on diffusion in nuclear fuels currently exist. Therefore, the aim of this work is to use atomistic simulation to investigate the diffusion of O^{2-} and U^{4+} in the region immediately surrounding dislocations and to discuss the implications for fuel behaviour.

2. Methodology

2.1. Modelling interactions in UO_2

The interactions between uranium and oxygen ions in UO_2 are represented using a combination of a long range Coulombic component, handled here using the direct summation method of Wolf et al. [17] and a short range empirical pair potential. Use of the direct summation has a number of advantages relative to the conventional Ewald summation [18]; principally it is computational less intensive and consequently allows the simulation of more ions but it is also known to be more effective for non-periodic systems such as dislocations [19].

There have been a large number of empirical pair potential parameter sets derived for the UO_2 system. Due to the large number of empirical potentials available there has been a significant effort to compare their relative performance [20–24]. Previous work has shown that 15 different empirical potential models predict the same ordering of the dislocation stability in UO_2 [25]. Here we adopt the potential model of Morelon et al. [26]. This potential has been widely employed to study diffusion in bulk UO_2 [27] and

* Corresponding author. Tel.: +44 (0)20 7594 6765.
E-mail address: samuel.murphy05@ic.ac.uk (S.T. Murphy).

0022-3115/$ - see front matter © 2014 Elsevier B.V. All rights reserved.
http://dx.doi.org/10.1016/j.jnucmat.2013.12.029

near grain boundaries [28,29] as well as for the study of dislocations [30,31], thereby allowing us to discuss the relative importance of pipe diffusion in UO_2.

2.2. Creating simulation supercells

The dislocation core structure may be generated either by displacing atoms according to linear elastic theory or via a 'misfit' approach such as that proposed by Bulatov and Cai [32]. Both methods have previously been applied to UO_2 [4,6,30,31]. Here we adopt a variation of the 'misfit' approach as described below.

For all dislocation systems studied here (a list is given Table 1) the ions are orientated such that the line direction of the dislocation lies along the z-axis and the Burgers vector lies along the y-axis. In all cases the Burgers vectors of the dislocations were chosen to be $\frac{1}{2}\langle 110\rangle$ in accordance with previous work [30]. Four dislocations were then created at $(x, y) = (0.25, 0.25)$, $(0.25, 0.75)$, $(0.75, 0.25)$ and $(0.75, 0.75)$ fractional co-ordinates by removing two planes of atoms between $(0.25, 0.25)$ and $(0.25, 0.75)$ and between $(0.75, 0.75)$ and $(0.75, 0.25)$, as shown in Fig. 1, and reducing the size of the supercell in the y-axis by a single Burgers vector. The supercell was then subjected to energy minimisation under constant volume conditions using the conjugate gradient algorithm in the LAMMPS simulation package [33]. By creating dislocations in this way we ensure that the number of planes of atoms in the y-axis remains constant across the entire supercell and consequently there is no unphysical strain at the periodic boundaries.

For a screw dislocation the Burgers vector is coincident with the line direction of the dislocation. In order to ensure that the screw dislocation is comparable to the edge dislocations the screw dislocation also had a Burgers vector of $\frac{1}{2}\langle 110\rangle$. Again the cell was oriented such that the line direction (and hence the Burgers vector) was aligned along the z-axis and four dislocations were then created at the same fractional co-ordinates as before by displacing the atoms by $u_z(x, y)$ according to linear elastic theory, i.e:

$$u_z(x, y) = \vec{b}\,\frac{\theta}{2\pi} \tag{1}$$

where θ is the angle between the ion and the dislocation core. The direction of the screw dislocations are set such that all neighbouring dislocations screw in opposite directions in order to ensure there are no spurious interactions at the cell boundaries.

2.3. Simulation procedure

For all simulations containing dislocations the supercells were chosen to have $x \simeq y \simeq 280$ Å, resulting in a separation between dislocations of $\simeq 140$ Å and a dislocation density of $\simeq 5.1 \times 10^{15}$ m^{-2}, which is only slightly greater than the dislocation density observed in high burn-up nuclear fuel [3]. In the z direction the cell was $\simeq$90 Å in order to achieve reliable statistics for the movement of ions surrounding the dislocations. The number of atoms in each supercell was in excess of 500,000.

Table 1
The proposed slip systems and Burgers vectors considered here as well as the specific vectors used.

Slip planes	Slip directions	Plane	Burgers vector	Line direction
{100}	⟨110⟩	(001)	$\frac{1}{2}[110]$	$[\bar{1}10]$
{110}	⟨110⟩	$(\bar{1}10)$	$\frac{1}{2}[110]$	[001]
{111}	⟨110⟩	$(\bar{1}11)$	$\frac{1}{2}[110]$	$[1\bar{1}2]$
Screw	⟨110⟩	–	$\frac{1}{2}[110]$	[110]

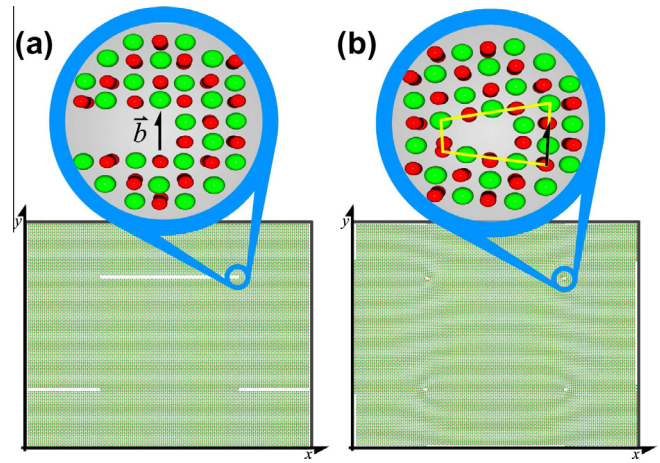

Fig. 1. Diagrammatic representation of the procedure for the creation of dislocations in UO_2. (a) The initial configuration with the two planes of atoms removed and (b) the supercell after energy minimisation. Clearly visible in (b) are the four $\frac{1}{2}\langle 110\rangle$ dislocations.

Diffusion in the vicinity of the dislocations was investigated using MD. The energy minimised supercells were equilibrated under constant pressure conditions using the Nose–Hoover thermo- and barostat at a series of temperatures between 1700 and 3200 K for 20 ps. A cylindrical region, of radius r, centred on the dislocation was defined and the mean-squared displacement (MSD) of the O^{2-} and U^{4+} ions within that cylinder was calculated over a period of up to 200 ps within the microcanonical (NVE) ensemble. The MSD may then be plotted as a function of time and the diffusivity, D, can be determined following Eq. (2):

$$D = \lim_{t\to\infty} \frac{1}{2d} \frac{\left[\vec{r_i}(t) - \vec{r_i}(t_0)\right]^2}{t} \tag{2}$$

where d is the dimensionality of the system and t is time. The gradient of the Arrhenius plot of the natural log of the diffusivity against $1/T$ is then E_a/k_B, where E_a is the activation energy, k_B is Boltzmann's constant and the diffusion coefficient can be determined from the intercept with the y-axis.

In order to compare the diffusion of O^{2-} and U^{4+} ions in the region immediately surrounding the dislocation and in the perfect lattice, the activation energies and diffusion coefficients have also been calculated in supercells of dislocation free UO_2. For these simulations the supercells were constructed from $20 \times 20 \times 20$ copies of the unitcell. The system was equilibrated for 10 ps under similar NPT conditions to those employed previously and then the MSD was monitored over a period of 20 ps.

3. Results

3.1. Structure of the {100}⟨110⟩ dislocation

For the {100}⟨110⟩ system there are a number of possible ionic configurations of the dislocation core that all exhibit the same Burgers vector [34]. Three different core configurations are investigated here; negatively charged, positively charged and charge neutral dislocation cores (shown in Fig. 2). These are compared by determining the line energy as a function of the distance from the dislocation core. Here the line energy, $E(r)$, is defined as the difference between the energy of the ions contained within a cylinder, $E_d(r)$, of radius, r, centred on the dislocation and the energy of an identical number of ions in the perfect lattice, $E_p(r)$, i.e:

$$E(r) = E_d(r) - E_p(r) \simeq E_d(r) - \sum_{j=U,O} N_j\langle E_j\rangle \tag{3}$$

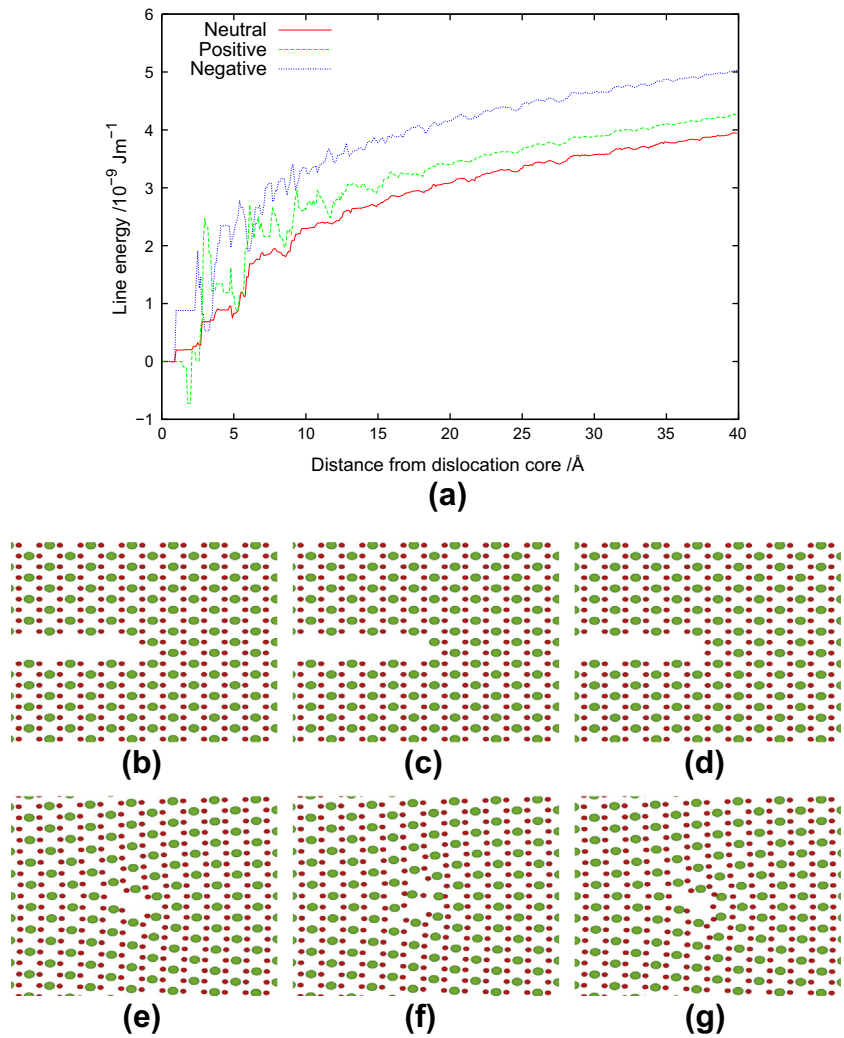

Fig. 2. Plot showing the line energies as a function of the distance from the dislocation core for the {100} dislocation. The charge neutral dislocation is shown with its unrelaxed structure in (b) and the final relaxed structure (e), similarly the positively charged dislocation core is shown before and after energy minimisation in (c) and (f) respectively. The negatively charged dislocation core is shown in (d) and (g) for the initial and final structures.

where N_j is the number of ions of each type j and $\langle E_j \rangle$ is the energy of ion j in bulk UO_2.

Fig. 2(a) shows the line energies for the different core configurations of the {100}⟨110⟩ dislocation after ions have reached their relaxed positions. The unrelaxed and relaxed configurations are shown in Figs. 2(b)-(d) and 2(e)-(g) respectively. The line energies shown in Fig. 2(a) predict that the charge neutral dislocation core has the lowest line energy of the possible {100}⟨110⟩ core structures and the negatively charged core has the highest energy. Due to the high mobility of the O^{2-} ions it is therefore expected that {100}⟨110⟩ dislocations in UO_2 will display the structure shown in Fig. 2(e) and therefore this is the only dislocation on the {100} slip plane considered below.

3.2. Dislocation stabilities

Fig. 3 shows the line energies of the four dislocations studied as a function of the distance from the dislocation core. Resulting line energies at 30 Å from the dislocation line are reported in Table 2. The line energies may be compared to values determined by Parfitt et al. [30] who created their initial dislocation geometries by displacing the atoms according to linear elastic theory. When displacing the atoms according to linear elastic theory the elastic constants of the material must be used to calculate the atomic displacements, however, in our approach dislocation structures are created by allowing the ions to relax according to the forces on the ions dictated by the potential model employed. Therefore, the elastic properties are inherent in the relaxation and the

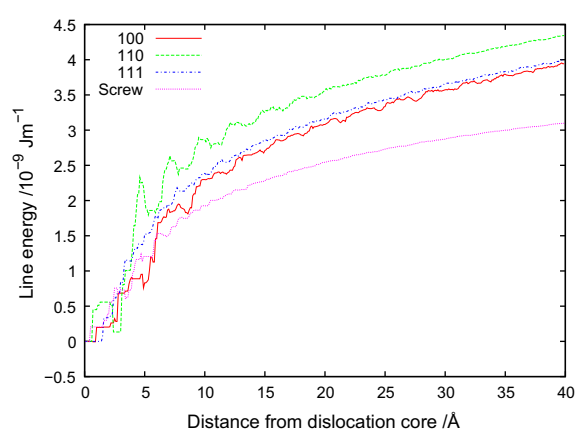

Fig. 3. Line energies for the dislocations studied here.

Table 2
Line energies at 30 Å from the dislocation core, D_0 and E_a for oxygen diffusion measured within 20 Å) compared to the dislocation free UO_2. The values given in brackets are the line energies calculated by Parfitt et al. [30], also at 30 Å, based on dislocation structures generated from linear elastic theory.

System	Line energy/Jm^{-1}	D_0/cm^2 s^{-1}	E_a /eV
Bulk UO_2	–	0.65	2.45
{100}⟨110⟩	3.57(3.51)	0.26	2.17
{110}⟨110⟩	4.01(4.19)	0.046	1.74
{111}⟨110⟩	3.66(3.75)	0.032	1.66
Screw	2.87(3.00)	0.048	1.75

dislocations generated should be similar to those predicted using linear elastic theory. The excellent level of quantitative agreement between the line energies at 30 Å calculated here and those reported by Parfitt et al. [30] provides further validation of the current method of generating dislocations. The ordering of the dislocation stabilities is also identical to that proposed by Fossati et al. [31] based on the stacking fault energies.

The screw dislocation is shown to have the lowest line energy and the {100}⟨110⟩ is predicted to be the most thermodynamically stable edge dislocation, closely followed by the {111}⟨110⟩ dislocation. This is in good agreement with the experimentally observed dominance of the {100}⟨110⟩ slip system [35].

3.3. Diffusion in bulk UO_2

Prior to an examination of diffusion surrounding a dislocation, diffusion of both anion and cations in the bulk was studied in order to provide frames of reference. The activation energy for O^{2-} diffusion was predicted to be 2.45 eV and the diffusion coefficient was predicted to be 0.65 cm^2 s^{-1}. These values are in excellent agreement with those of Govers et al. [27], which were calculated using the same methodology and empirical pair potential. No diffusion of U^{4+} was observed in the simulations of bulk UO_2.

3.4. Diffusion near dislocations

The range over which the dislocation can affect the rate of diffusion was examined by calculating the activation energies in a series of concentric regions centred on the dislocation. Initially the activation energy was calculated in an innermost core region, which contained all O^{2-}/U^{4+} ions within 5 Å of the dislocation, the next region considered all O^{2-}/U^{4+} ions between 5 and 10 Å from the core and so on up to a radius of 35 Å.

The influence of the distance from the dislocation on the activation energies for diffusion were investigated for the {110}⟨110⟩ edge and screw dislocations and the results are shown in Fig. 4. Also shown in Fig. 4 is the activation energy for O^{2-} diffusion in the bulk (dotted line). The results show that there is indeed a significant reduction in the activation energies for diffusion close to the dislocations. The change in the activation energies for O^{2-} diffusion are very similar for the {110}⟨110⟩ and screw dislocations. As the distance from the dislocation core increases there is a steady increase in the calculated activation energies and the bulk activation energy has been recovered at a distance of 20 Å. Therefore, in further studies the quoted activation energies for O^{2-} diffusion relates to ions within 20 Å of the dislocation only. Around the screw dislocation there was evidence of some U^{4+} diffusion, however, it was not sufficient to accurately determine an activation energy. By contrast around the {110}⟨110⟩ edge dislocation the activation energy for diffusion increased from 1.57 eV at 5 Å to 5.45 eV between 10 and 15 Å. Outside of this region no diffusion was observed.

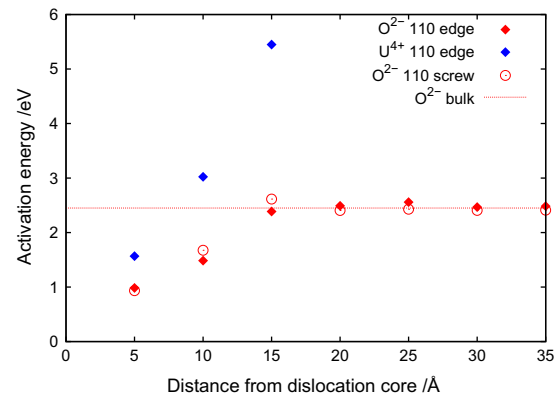

Fig. 4. Activation energy for diffusion as a function of the distance from the {110}⟨110⟩ edge and screw dislocation cores. The plot shows that close to the dislocation core the activation energies for O^{2-} and U^{+4} are decreased, however at separations > 20 Å the activation energy for oxygen diffusion is similar to that expected in the bulk (horizontal red line in the plot), however, for uranium there is no diffusion observed at distances > 15 Å from the {110}⟨110⟩ edge dislocation.

During the simulations there were a number of ions that were able to enter the core of the dislocation and move rapidly along the dislocation line, however, most of the increased diffusion occurs in the tensile region of the dislocation strain field, while there appears to be reduced diffusion within the compressive region. In the tensile region the ions are slightly further apart than in the bulk and so it would be expected that the activation energy for an ion to move between ions would be reduced. By contrast, in the compressive region the converse would be expected with the ions being closer together resulting in higher activation energies. Simulations of strained CeO_2 show that this effect is not isotropic and that the increase in oxygen diffusivity in the bulk under tension is greater than the reduction in diffusivity observed when the same amount of compressive strain is applied [36]. These observations of strained bulk crystals suggest that the introduction of an edge dislocation with approximately equal regions of compressive and tensile strain (the strain fields surrounding edge dislocations are given in Parfitt et al. [30]) should lead to an overall increase in the diffusivity. The difference in the diffusion of U^{4+} close to {110}⟨110⟩ and screw dislocations can be ascribed to the lack of any highly tensile regions in the strain field surrounding the screw dislocation that are present close to the core of the {110}⟨110⟩ edge dislocation.

Next we compare oxygen ion diffusion surrounding the different dislocations studied here. We note that as the temperature is increased the dislocations themselves become mobile and are observed to move several lattice spacings during the course of the simulations. The most significant slip was observed in the {100}⟨110⟩ and {111}⟨110⟩ systems where the predicted Peierls barriers are the lowest and consequently these dislocations would be expected to be the most mobile [30]. The MSD's were carefully monitored to ensure that the movement of the dislocations did not influence the calculated activation energies and diffusion coefficients. The dislocation movement was not found to have any significant impact on O^{2-} diffusion, however, due to the small total distances travelled by the U^{4+} ions, even at very high temperatures, the contribution to the MSD due to dislocation slip is significant.

Fig. 5 and Table 2 show that for all dislocations there is a significant reduction in the activation energies and diffusion coefficients for O^{2-} diffusion in the region immediately surround a dislocation, however, the activation energies are not the same for all dislocations. The activation energy for O^{2-} diffusion in the vicinity of the {100}⟨110⟩ dislocation was reduced by the least (i.e. to 2.17 eV compared to 2.45 eV in bulk UO_2), while for the other edge

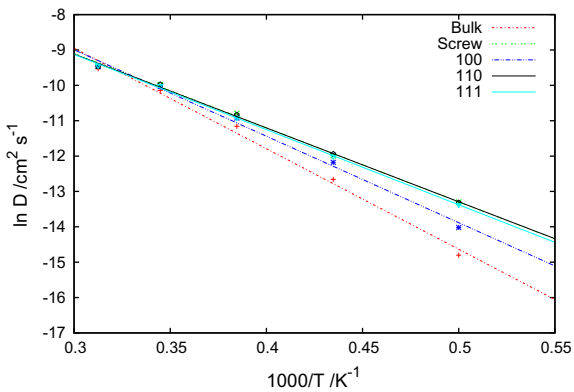

Fig. 5. Arrhenius plot showing the logarithm of D as a function of 1000/T for all the different dislocations studied here. For comparison similar data is also shown for oxygen diffusion in the bulk UO_2.

dislocations the activation energies range from 1.66 to 1.75 eV. In comparison the $\{100\}\langle 110\rangle$ core is more compact and consequently there is less room for the O^{2-} ions to move through the core. Additionally, the strain field is smaller thus reducing the range over which the dislocation can enhance diffusion. However, the screw dislocation while exhibiting the lowest line energy exhibits a much reduced activation energy. This may be a consequence of the different strain field for a screw dislocation (quadrapolar) compared to that for an edge dislocation (dipolar). This observation of different levels of O^{2-} diffusion surrounding the different dislocations is commensurate with different levels of oxygen defects surrounding the core region [31].

The MSD's calculated for U^{4+} were found to be very small even in the core region of the dislocations. For the $\{100\}\langle 110\rangle$ and $\{111\}\langle 110\rangle$ edge dislocations the high temperatures required to initiate uranium diffusion also activate slip. The contribution of this slip to the U^{4+} MSD's is significant and so cannot be considered as pipe diffusion. By contrast the $\{110\}\langle 110\rangle$ system has a high Peierls barrier [30] and consequently it is possible to examine U^{4+} diffusion around the dislocation.

In order to investigate the diffusion mechanisms in the region surrounding the dislocation the self-part of the van Hove space time auto-correlation functions were determined [37]. The van Hove auto-correlation function highlights the dynamical correlations of the atom trajectories and defines the probability that an ion at its origin at $t = 0$ will have travelled a distance, dr, at time t. This is more formally expressed as:

$$G_{self}(\vec{r},t) = \frac{1}{N}\left\langle \sum_{i=1}^{N} \delta[\vec{r} + \vec{r}_i(0) - \vec{r}_i(t)] \right\rangle \tag{4}$$

where $G_{self}(\vec{r},t)$ is the probability that an atom i has moved a distance r in a time, t, N is the number of atoms, $\vec{r}_i(0)$ is the initial position of atom i and $\vec{r}_i(t)$ corresponds to the position of i at time t. The brackets denote a statistical average over different configurations. Auto-correlation functions were determined for O^{2-} self diffusion within 20 Å of the dislocation at 1700 K for t = 15 ps.

The van Hove auto-correlation functions for the $\{110\}\langle 110\rangle$, $\{100\}\langle 110\rangle$ and screw dislocations are plotted in Fig. 6. Also included in Fig. 6 are the partial van Hove auto-correlation functions where G_{self} is determined in x, y and z independently for the same dislocations. Fig. 6(f) shows that the majority of ions have not left their initial lattice sites, hence the large peak at ≈ 1 Å. The second peak at ≈ 3.5 Å corresponds to the probability of an atom hoping to a nearest neighbour site. Beyond this the total van Hove functions (Fig. 6(a)–(c)) appear to have no clearly defined peaks, which suggests a more Brownian type of motion rather than a hopping mechanism as would be expected in a crystal. However, by examining the partial van Hove auto-correlation functions (Fig. 6(f)) it is evident that there are clearly defined peaks representing hops between well defined sites except in the region 4–6 Å in y for the $\{110\}\langle 110\rangle$ and $\{100\}\langle 110\rangle$ dislocations. This region of ill defined peaks in the y directions is due to ions traversing the core of the dislocation where there are no clearly defined lattice sites. It is also noteworthy that the probability of atoms moving larger distances is greater for the $\{110\}\langle 110\rangle$ and screw dislocations, which would be anticipated from Fig. 5 because they exhibit lower activation energies.

4. Discussion

A simple model for dislocation assisted diffusion, D_a, is presented in Eq. (5) [38]:

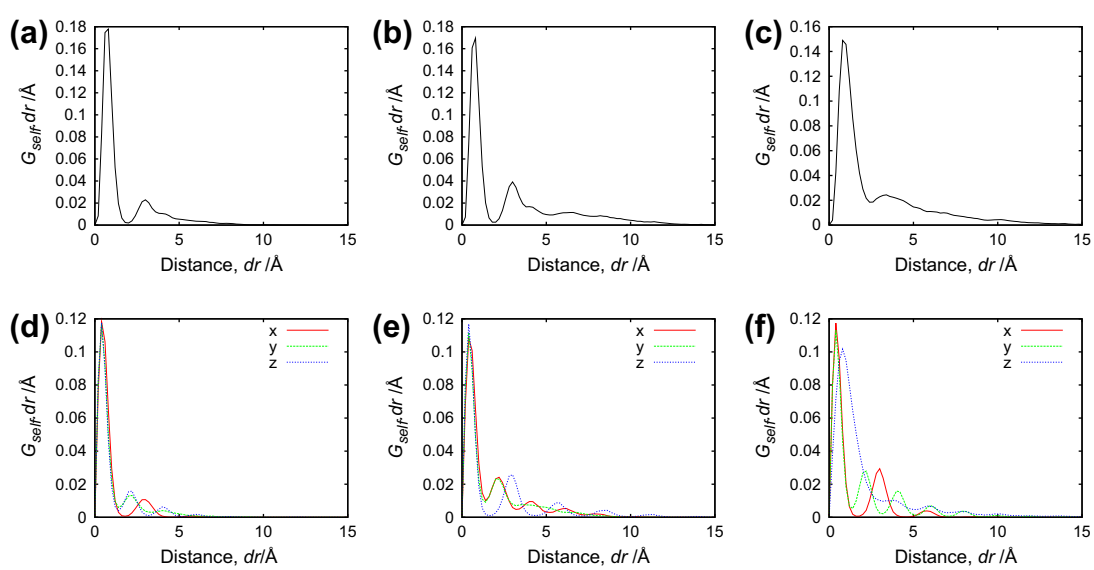

Fig. 6. Full and partial van Hove auto-correlation functions for oxygen atoms within 20 Å of the $\{100\}\langle 110\rangle$ dislocation (figures (a) and (d)), $\{110\}\langle 110\rangle$ dislocation (figures (b) and (e)) and screw dislocations (figures (c) and (f)).

$$D_a = D_b(1-f) + D_d f \quad (5)$$

where D_b and D_d are the diffusion coefficients for bulk UO_2 and the dislocation core respectively and f is the fraction of diffusing species that undergo pipe diffusion. Assuming the number of atoms per unit volume is equal to that in the bulk then f is simply the product of the dislocation density and the cross sectional area of the core. Shown in Fig. 7 is a plot of $\log(D_a/D_b)$ for oxygen as a function of temperature for the different dislocations studied at a dislocation density of 1×10^{15} m^{-2}. Fig. 7 shows that at low temperatures, with the exception of the $\{100\}\langle110\rangle$ dislocation, there is a considerable enhancement in the overall oxygen diffusivity due to the presence of the dislocations. This effect decreases rapidly as the temperature is increased, although it may still be significant at the rim of fuel pellet (prior to the formation of the HBS at which point the dislocation density is dramatically reduced) where temperatures can be ≈800 K [39] or under storage conditions. An enhancement of approximately one order of magnitude is predicted at 1000 K as has been observed for albite [40].

Presented in Table 3 are the migration energies for the intrinsic point defects in UO_2 calculated using nudged elastic band simulations [41] with the Morelon potential and density functional theory. The activation energies for oxygen interstitial and vacancy migration are shown to be lower than those calculated close to the dislocation core.

Since no uranium diffusion was observed in the bulk UO_2 it is not possible to determine D_a, however, it is again instructive to compare the activation energies calculated in the dislocation core and the migration energies of the isolated point defects. The activation energy of 1.57 eV in the core of the dislocation is significantly lower than the migration energy for either the uranium vacancy (4.2 eV) or interstitial defects (3.9 eV). Consequently, the results suggest that dislocation assisted diffusion will play an important role in U^{4+} transport. As shown previously the diffusion rate of some fission products, and in particular Xe, may be dictated by migration on the uranium sublattice. Therefore, these results may help explain the enhanced diffusion of Xe observed at temperatures < 1300 °C [12].

At elevated temperatures the high rate of diffusion of gas atoms to traps (e.g. bubbles) is expected to overwhelm fission gas re-solution processes [44,45]. As a consequence, the fuel grains should retain their fission gas inventory. Experimental observations, by contrast, suggest that during a transient the release rate of fission gas is increased. Two mechanisms have been proposed to explain this phenomena, the first is thermal resolution from the bubbles and the second is enhanced fission gas migration from the fuel grain, with dislocations providing the pathway for this enhanced diffusion [44,46]. The results presented here suggest that dislocations are indeed capable of providing a pathway for the increased diffusion on the uranium sublattice and possibly enhancing the diffusion of fission gasses.

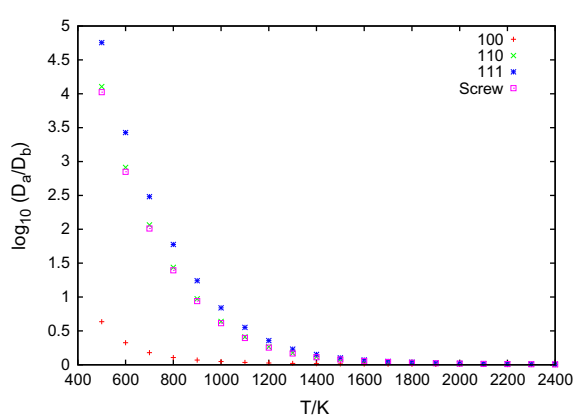

Fig. 7. Plot showing the enhancement in the total diffusivity of oxygen by pipe diffusion at to a dislocation density of 1×10^{15} m^{-2} for our four dislocations as a function of temperature.

Table 3
Table showing the migration energies for the interstitial and vacancy defects in UO_2.

Defect	Migration energy/eV	
	Morelon (Govers et al.[20])	Dorado et al. [42,43]
O_i-interstitialcy	0.7	0.93
O_i-direct	0.7	3.22
V_O	0.67	0.3
U_i	3.9	4.2
V_U	4.2	4.4

5. Conclusions

We have proposed a variation of the 'misfit' approach [32] for the generation of dislocations in MD simulations. The resulting supercells contain four dislocations arranged such that their displacement fields cancel out, ensuring no spurious strains at the periodic boundaries. The line energies for the dislocations are in excellent agreement with similar results calculated for dislocations generated by displacing the ions according to linear elastic theory [30].

In the region immediately surrounding the centre of the dislocation the activation energies and diffusion coefficients for both O^{2-} and U^{4+} are significantly reduced relative to the bulk UO_2 lattice. This indicates that dislocations enhance diffusion by pipe diffusion. The extent of the region in which the diffusion is enhanced is relatively small; it extends only to a distance of 15–20 Å from the centre of dislocation. Nevertheless, even within 5 Å of the dislocation core the activation energy is greater than for diffusion predicted at grain boundaries [28]. The degree of enhancement due to pipe diffusion is strongly dependent on the structure of the dislocation core with the most thermodynamically stable $\{100\}\langle110\rangle$ edge dislocation showing the smallest reduction in the activation energy and diffusion coefficient for oxygen diffusion due to its compact core structure. Conversely, the screw dislocation shows significantly enhanced oxygen diffusion despite having the lowest line energy, which may be related to the different strain field surrounding this dislocation.

In a real nuclear fuel it is not expected that pipe diffusion will make a significant contribution to the overall oxygen diffusivity at high temperatures, however it may be significant at lower temperatures. By contrast, for uranium the introduction of dislocations leads to a significant decrease in the activation energy close to the dislocation core relative to diffusion mediated by point defects. This increase in the mobility has significant implications for the diffusivity of fission gas species that may segregate to the dislocation [7] as the activation energy for U^{4+} is predicted to be the rate determining step for Xe migration.

Acknowledgements

All calculations were performed using the Imperial College High Performance Computing Service. STM would like acknowledge fund from EPSRC under contract (EN20100200) and EEJ would like to acknowledge funding from the CASL consortium. Laurent van Brutzel is thanked for useful conversations and Edoardo Giorgi is thanked for help with the images.

References

[1] G.S. Was, Fundamentals of Radiation Materials Science, Springer-Verlag, Heidelberg, 2007.
[2] R. Devanathan, L. Van Brutzel, A. Chartier, C. Gueneau, A.E. Mattsson, V. Tikare, T. Bartel, T. Besmann, M. Stan, P. Van Uffelen, Energy Environ. Sci. 3 (2010) 1406.
[3] K. Nogita, K. Une, Nucl. Inst. Methods Phys. Res. B – Beam Interact. Mater. Atoms 91 (1994) 301.
[4] B. Deng, A. Chernatynskiy, P. Shukla, S.B. Sinnott, S.R. Phillpot, J. Nucl. Mater. 434 (2013) 203.
[5] C. Baker, J. Nucl. Mater. 66 (1977) 283.
[6] A. Goyal, T. Rudzik, B. Deng, M. Hong, A. Chernatynskiy, S.B. Sinnott, S.R. Phillpot, J. Nucl. Mater. 441 (2013) 96.
[7] P.V. Nerikar, D.C. Parfitt, L.A. Casillas Trujillo, D.A. Andersson, C. Unal, S.B. Sinnott, R.W. Grimes, B.P. Uberuaga, C.R. Stanek, Phys. Rev. B 84 (2011) 174105.
[8] V.V. Rondinella, T. Wiss, Mater. Today 13 (2010) 24.
[9] J. Jonnet, B. Remy, P. Van Uffelen, Theor. Appl. Frac. Mech. 45 (2006) 238.
[10] T. Sonoda, M. Kinoshita, I.L.F. Ray, H. Wiss, T. Thiele, D. Pellottiero, V.V. Rondinella, H. Matzke, Nucl. Instrum. Meth. B 191 (2002) 622.
[11] K. Otsuka, A. Kuwabara, A. Nakamura, T. Yamamoto, K. Matsunaga, Y. Ikuhara, Appl. Phys. Lett. 82 (2003) 877.
[12] R.M. Cornell, J. Nucl. Mater. 38 (1971) 319.
[13] X. Zhang, G. Lu, Phys. Rev. B 82 (2010) 012101.
[14] Q.F. Fang, R. Wang, Phys. Rev. B 62 (2000) 9317.
[15] R.C. Picu, D. Zhang, Acta Mater. 52 (2004) 161.
[16] F. Chang, A.M. Walker, K. Wright, J.D. Gale, J. Mater. Chem. 20 (2010) 10445.
[17] D. Wolf, P. Keblinski, S.R. Phillpot, J. Eggebrecht, J. Chem. Phys. 110 (1999) 8254.
[18] P.P. Ewald, Ann. Phys. 369 (3) (1921) 524.
[19] E.E. Gdoutos, R. Agrawal, H.D. Espinosa, Int. J. Numer. Meth. Eng. 84 (2010) 1541.
[20] K. Govers, S. Lemehov, M. Hou, M. Verweft, J. Nucl. Mater. 366 (2007) 161.
[21] K. Govers, S. Lemehov, M. Hou, M. Verweft, J. Nucl. Mater. 376 (2008) 66.
[22] R. Devanathan, J.G. Yu, W.J. Weber, J. Chem. Phys. 130 (2009) 174502.
[23] S.I. Potashnikov, A.S. Boyarchenkov, K.A. Nekrasov, A.Y. Kupryazhkin, J. Nucl. Mater 419 (2011) 217.
[24] A. Chernatynskiy, C. Flint, S.R. Sinnott, S.B. Phillpot, J. Mater. Sci. 47 (2012) 7693.
[25] S.T. Murphy, M.J.D. Rushton, R.W. Grimes, Prog. Nucl. Energy http://dx.doi.org/10.1016/j.pnucene.2013.09.010.
[26] N.D. Morelon, D. Ghaleb, J.M. Delaye, L. Van Brutzel, Philos. Mag. 83 (13) (2003) 1533.
[27] K. Govers, S. Lemehov, M. Hou, M. Verweft, J. Nucl. Mater. 395 (2009) 131.
[28] E. Vincent-Aublant, J.-M. Delaye, L. Van Brutzel, J. Nucl. Mater. 392 (2009) 114.
[29] K. Govers, M. Verweft, J. Nucl. Mater. 438 (2013) 134.
[30] D.C. Parfitt, C.L. Bishop, M.R. Wenman, R.W. Grimes, J. Phys.: Condens. Mater. 22 (2010) 175004.
[31] P. Fossati, L. Van Brutzel, B. Devincre, J. Nucl. Mater http://dx.doi.org/10.1016/j.jnuc.mat.2013.07.059.
[32] V.V. Bulatov, W. Cai, Computer Simulations of Dislocations, Oxford University, Oxford, 2006.
[33] S. Plimpton, J. Comput. Phys. 117 (1995) 1.
[34] A.G. Evans, P.L. Pratt, Philos. Mag. 20 (1969) 1213.
[35] R.J. Keller, T.E. Mitchell, A.H. Heuer, Acta Metal. 36 (1988) 1073.
[36] M.J.D. Rushton, A. Chroneos, S.J. Skinner, J.A. Kilner, R.W. Grimes, Solid State Ionics 230 (2013) 37.
[37] L. van Hove, Phys. Rev. 95 (1954) 249.
[38] E.W. Hart, Acta Metall. 5 (1957) 597.
[39] H. Bailly, D. Menessier, C. Prunier, The Nuclear Fuel of Pressurized Water Reactors and Fast Neutron Reactors, Lavoisier Publishing, Paris, 1999.
[40] R.A. Yund, B.M. Smith, J. Tullis, Phys. Chem. Min. 7 (1981) 185.
[41] G. Henkelman, B.P. Uberuaga, H. Jonsson, J. Chem. Phys. 113 (2000) 9901.
[42] B. Dorado, D.A. Andersson, C.R. Stanek, M. Bertolus, B.P. Uberuaga, G. Martin, M. Freyss, P. Garcia, Phys. Rev. B 86 (2012) 035110.
[43] B. Dorado, P. Garcia, G. Carlot, C. Davoisne, M. Fraczkiewicz, B. Pasquet, M. Freyss, C. Valot, G. Baldinozzi, D. Simeone, M. Bertolus, Phys. Rev. B 83 (2011) 035126.
[44] J. Shea, An extension to fission gas release modelling at high temperatures, EHPG Storefjell, 2013.
[45] C.T. Walker, M. Mogensen, J. Nucl. Mater. 149 (1987) 121.
[46] Szuta, IAEA TECDOC-1233 77.